# Simultaneous type I and type II Čerenkov-phase matched second-harmonic generation in disordered nonlinear photonic structures

**Mousa Ayoub,* Markus Paßlick, Jörg Imbrock, and Cornelia Denz**

*Institute of Applied Physics and Center for Nonlinear Science (CeNoS), Westfälische Wilhelms-Universität Münster, Corrensstraße 2, 48149 Münster, Germany*

*ayoubm@uni-muenster.de

**Abstract:** We observe simultaneous type I and II Čerenkov-phase matched second-harmonic generation in a disordered nonlinear photonic crystal. The mean width of the disordered ferroelectric domains and the laser beam width are adjusted to be on the same length scale. We analyze the polarization properties, emission angles and intensities of each process.



**OCIS codes:** (190.0190) Nonlinear optics; (190.4410) Nonlinear optics, parametric processes; (190.4975) Parametric processes; (160.2260) Ferroelectrics.

## References and links

1. A. R. Tunyagi, M. Ulex, and K. Betzler, "Noncollinear optical frequency doubling in strontium barium niobate," Phys. Rev. Lett. **90**, 243901 (2003).
2. R. Fischer, S. M. Saltiel, D. N. Neshev, W. Krolikowski, and Y. S. Kivshar, "Broadband femtosecond frequency doubling in random media," Appl. Phys. Lett. **89**, 191105 (2006).
3. X. Vidal and J. Martorell, "Generation of light in media with a random distribution of nonlinear domains," Phys. Rev. Lett. **97**, 013902 (2006).
4. P. Molina, M. de la O Ramírez, and L. E. Bausá, "Strontium barium niobate as a multifunctional two-dimensional nonlinear photonic glass," Adv. Funct. Mater. **18**, 709–715 (2008).
5. A. M. Vyunishev, A. S. Aleksandrovsky, A. I. Zaitsev, and V. V. Slabko, "Čerenkov nonlinear diffraction in random nonlinear photonic crystal of strontium tetraborate," Appl. Phys. Lett. **101**, 211114 (2012).
6. N. An, Y. Zheng, H. Ren, X. Deng, and X. Chen, "Conical second harmonic generation in one-dimension nonlinear photonic crystal," Appl. Phys. Lett. **102**, 201112 (2013).
7. V. Vaičaitis, "Cherenkov-type phase matching in bulk KDP crystal," Opt. Commun. **209**, 485–490 (2002).
8. K. A. Kuznetsov, G. K. Kitaeva, A. V. Shevlyuga, L. I. Ivleva, and T. R. Volk, "Second harmonic generation in a strontium barium niobate crystal with a random domain structure," JETP Lett. **87**, 98–102 (2008).
9. Y. Sheng, V. Roppo, Q. Kong, K. Kalinowski, Q. Wang, C. Cojocaru, J. Trull, and W. Krolikowski, "Tailoring Čerenkov second-harmonic generation in bulk nonlinear photonic crystal," Opt. Lett. **36**, 2593–2595 (2011).
10. M. Ayoub, P. Roedig, J. Imbrock, and C. Denz, "Domain-shape-based modulation of Čerenkov second-harmonic generation in multidomain strontium barium niobate," Opt. Lett. **36**, 4371–4373 (2011).
11. M. Ayoub, P. Roedig, J. Imbrock, and C. Denz, "Cascaded Čerenkov third-harmonic generation in random quadratic media," Appl. Phys. Lett. **99**, 241109 (2011).
12. W. Wang, Y. Sheng, Y. Kong, A. Arie, and W. Krolikowski, "Multiple Čerenkov second-harmonic waves in a two-dimensional nonlinear photonic structure," Opt. Lett. **35**, 3790–3792 (2010).
13. H. X. Li, S. Y. Mu, P. Xu, M. L. Zhong, C. D. Chen, X. P. Hu, W. N. Cui, and S. N. Zhu, "Multicolor cerenkov conical beams generation by cascaded-$\chi^{(2)}$ processes in radially poled nonlinear photonic crystals," Appl. Phys. Lett. **100**, 101101 (2012).
14. N. An, Y. Zheng, H. Ren, X. Zhao, X. Deng, and X. Chen, "Normal, degenerated, and anomalous-dispersion-like cerenkov sum-frequency generation in one nonlinear medium," Photonics Res. **3**, 106–109 (2015).
15. Y. Sheng, A. Best, H.-J. Butt, W. Krolikowski, A. Arie, and K. Koynov, "Three-dimensional ferroelectric domain visualization by Čerenkov-type second harmonic generation," Opt. Express **18**, 16539–16545 (2010).

#247476 Received 6 Aug 2015; revised 25 Sep 2015; accepted 27 Sep 2015; published 21 Oct 2015

16. P. Karpinski, X. Chen, V. Shvedov, C. Hnatovsky, A. Grisard, E. Lallier, B. Luther-Davies, W. Krolikowski, and Y. Sheng, "Nonlinear diffraction in orientation-patterned semiconductors," Opt. Exp. **23**, 14904–14912 (2015).
17. S. M. Saltiel, Y. Sheng, N. Voloch-Bloch, D. N. Neshev, W. Krolikowski, A. Arie, K. Koynov, and Y. S. Kivshar, "Cerenkov-type second-harmonic generation in two-dimensional nonlinear photonic structures," IEEE J. Quantum Electron. **45**, 1465–1472 (2009).
18. K. Kalinowski, P. Roedig, Y. Sheng, M. Ayoub, J. Imbrock, C. Denz, and W. Krolikowski, "Enhanced Čerenkov second-harmonic emission in nonlinear photonic structures," Opt. Lett. **37**, 1832–1834 (2012).
19. A. Fragemann, V. Pasiskevicius, and F. Laurell, "Second-order nonlinearities in the domain walls of periodically poled $KTiOPO_4$," Appl. Phys. Lett. **85**, 375–377 (2004).
20. Y. Sheng, V. Roppo, K. Kalinowski, and W. Krolikowski, "Role of a localized modulation of $\chi^{(2)}$ in čerenkov second-harmonic generation in nonlinear bulk medium," Opt. Lett. **37**, 3864–3866 (2012).
21. Y. Sheng, Q. Kong, V. Roppo, K. Kalinowski, Q. Wang, C. Cojocaru, and W. Krolikowski, "Theoretical study of Čerenkov-type second-harmonic generation in periodically poled ferroelectric crystals," J. Opt. Soc. Am. B **29**, 312–318 (2012).
22. M. Ayoub, J. Imbrock, and C. Denz, "Second harmonic generation in multi-domain $\chi^2$ media: from disorder to order," Opt. Express **19**, 11340–11354 (2011).
23. S. Podlozhenov, H. A. Graetsch, J. Schneider, M. Ulex, M. Wöhlecke, and K. Betzler, "Structure of strontium barium niobate $Sr_xBa_{1-x}Nb_2O_6$ (SBN) in the composition range $0.32 \leq x \leq 0.82$," Acta Cryst. **B62**, 960–965 (2006).
24. F. Sibbers, J. Imbrock, and C. Denz, "Sum-frequency generation in disordered quadratic nonlinear media," Proc. SPIE **7728**, 77280Y (2010).
25. T. Woike, T. Granzow, U. Dörfler, C. Poetsch, M. Wöhlecke, and R. Pankrath, "Refractive indices of congruently melting $Sr_{0.61}Ba_{0.39}Nb_2O_6$," Phys. Stat. Sol. A **186**, R13 (2001).

## 1. Introduction

The broadband frequency conversion in nonlinear photonic crystals (NLPC) of random distribution of the $\chi^{(2)}$-nonlinearity has recently attracted much attention [1–6]. Čerenkov-type second-and third-harmonic noncollinear emissions are one of the most interesting patterns in far-field because of its spatial properties and spectral dependencies [7–14], and potential applications in microscopy [15, 16]. The spatial properties of Čerenkov emission for both SH- and TH emissions have been already studied. In general, the Čerenkov emission is observable when fulfilling the corresponding longitudinal phase-matching condition, i.e. when the longitudinal phase-mismatch is zero [cf. Fig 1(a)] : $\cos\theta_c = (k_{o/e}^{(\omega)} + k_{o/e}^{(\omega)})/k_{o/e}^{(2\omega)}$, where $\theta_c$ is the Čerenkov opening angle, $k^{(\omega)}$ and $k^{(2\omega)}$ are the wave vectors of the fundamental and second harmonic waves, respectively. This kind of phase-matching condition is considered as a special case of the noncollinear Bragg phase-matching condition. In 2D NLPC it takes a conical form and experiences particular modulation, which can be attributed either to the individual domain shape corresponding to the crystal symmetry or to the polarization properties of the $\chi^2$ tensor or to both [10, 17]. The polarization properties of Čerenkov emission differ depending on the propagation direction with respect to the optical axis of the crystal and of-course on the crystal symmetry. For example, for propagating along the optical axis, Čerenkov emission is radially polarized in SBN, and both radially and azimuthally polarized in $LiNbO_3$. Moreover, experiments to enhance the generation efficiency, based on the contribution of the reciprocal grating vectors, in both 1D and 2D periodically poled $\chi^2$ media have been recently successfully performed [18]. However, the physical origin of this phenomenon is still unclear, being caused either by strong nonlinearities on the domain walls [19] or by the broad spectra of reciprocal vectors [15, 17], although the phase-matching condition for this effect does not exhibit dependencies to reciprocal vectors. A recent study has proved that the sharp modulation of the $\chi^{(2)}$-nonlinearity constitutes a sufficient condition for the emission of Čerenkov second harmonic in bulk materials [20]. Moreover, effect of the strength of the emitted Čerenkov harmonic signal and the sensitivity of the emission process to wavelength tuning have also been investigated [21].

In this paper, we report on three emission possibilities of Čerenkov second-harmonic gen-

#247476 Received 6 Aug 2015; revised 25 Sep 2015; accepted 27 Sep 2015; published 21 Oct 2015

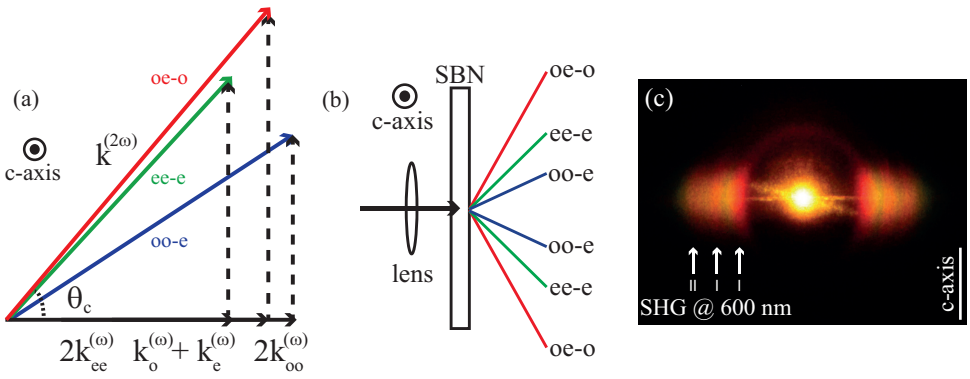


Fig. 1. (a) The phase-matching condition for the three processes allowed by the $\chi^2$ tensor. (b) Schematic of the Čerenkov signal measurements. (c) An experimental photograph of the three Čerenkov-phase matched second harmonics of 1200 nm. The fundamental wave in (c) is linearly polarized at an angle of 45° with respect to the c-axis.

eration in a multi-domain strontium barium niobate (SBN), indicating three processes allowed by the $\chi^2$ tensor, namely: Type I: $e+e \rightarrow e$, $o+o \rightarrow e$, and Type II: $o+e \rightarrow o$. Čerenkov SHG in random SBN is typically observed when the fundamental wave propagates along the optical axis. However, in this case only one nonlinear process can be observed, namely $o+o \rightarrow e$. We analyze the opening angle over a wide wavelength range and the polarization state of the individual Čerenkov emissions, when the fundamental wave propagates perpendicularly to the optical axis. In this configuration the Čerenkov signal is always present, but covered by the transverse emission caused by the broad spectrum of reciprocal vectors [22]. Thus, up to now all three Čerenkov phase-matched SHG processes have not been measured in this configuration.

## 2. Experimental methods

### *2.1. Preparation and characterization of ferroelectric domains*

As well known, SBN crystals are of 4mm symmetry [23]. The ferroelectric domains are needle-like with cross sections of squares with rounded corners [10] and randomly distributed as seen in Fig. 2. The domain size distribution can be effectively controlled by applying an electric field along the crystallographic axis of the crystal [22], or by heating-up over Curie temperature followed by cooling down to room temperature. As a result, SBN crystal can have different average domain sizes beginning from $\approx$ 300 nm for the cooled-down case as in Figs. 2(b) and 2(c) to several tens of micrometers for the repoled case [22] [see Figs. 2(d) and 2(e)]. To characterize the domain sizes we have imaged the domains using a laser scanning microscope similar to that in [15]. Femtosecond laser pulses with a wavelength of 800 nm and a repetition rate of 80 MHz are focused by a microscope objective with a numerical aperture of 1.49 to a diffraction limited spot size with a width of about 500 nm [see Fig. 2(a)]. The sample is scanned with a piezo-table in all three dimensions with a step size of 500 nm. When the laser focus hits a domain wall second-harmonic waves are emitted at the Čerenkov angles whereas no second harmonic is generated in a crystal volume with a homogeneous $\chi^{(2)}$-nonlinearity. The generation of Čerenkov SHG at a domain wall can explained in the framework of the phase-matching condition. At Čerenkov angle, which is only determined by the refractive indices of the fundamental and harmonic waves, the longitudinal phase-mismatch is zero. The transversal phase mismatch is partially compensated for by a wave vector that is nonzero due to the Fourier

#247476 Received 6 Aug 2015; revised 25 Sep 2015; accepted 27 Sep 2015; published 21 Oct 2015

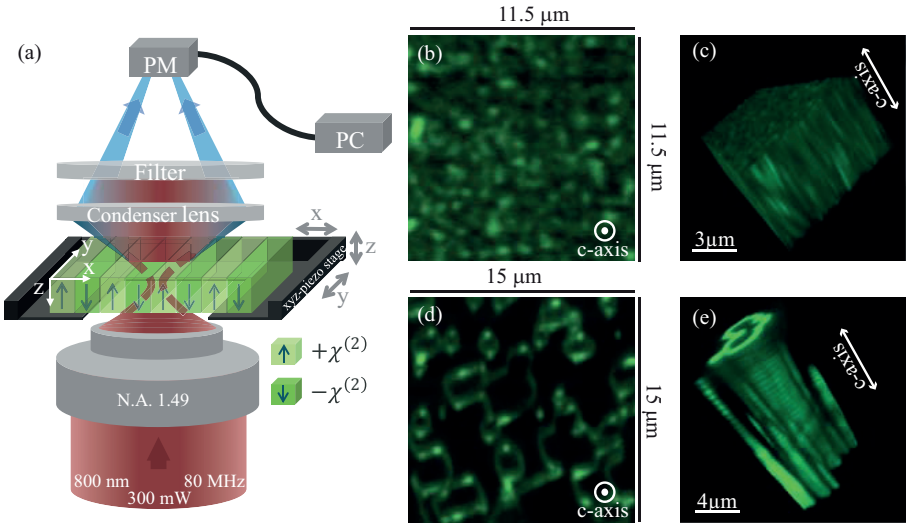


Fig. 2. (a) Schematic of the experimental microscope; PM:Photomultimeter, M.O.: Microscope objective, PC: Computer. (b) and (d) Čerenkov-type SHG microscopy images of ferroelectric domains in SBN perpendicular to the optical axis in different size scales. (c) and (e) Three dimensional visualization of isolated ferroelectric domains inside randomized SBN in different size scales (see Visualization 1 and Visualization 2).

spectrum of the domain wall [20]. In our Čerenkov SHG microscope the fundamental wave always propagates along the optical axis which leads to one Čerenkov phase-matched SHG process $o+o \rightarrow e$. Figures 2(d) and 2(e) show a random distribution of ferroelectric domains in SBN after applying an electric field above the coercive field of about 2.5 kV/cm several times parallel and anti-parallel to the optical axis. The green lines in Figs. 2(b)–2(e) correspond to domain walls. We can change the mean domain width between hundreds of nanometers and a few micrometers.

### *2.2. Čerenkov type I and II SHG analyzing setup*

To observe type I and II Čerenkov-phase matched SHG we use ultrashort laser pulses, generated by a laser system consisting of a mode-locked Ti:sapphire oscillator, a regenerative amplifier and an optical parametric amplifier. The repetition rate is 1 kHz, the pulse duration is about $\tau_p = 80$ fs, and the pulse energies are up to 100 µJ depending on the wavelength which can be tuned between 470 nm and 2700 nm. A lens was used to loosely focus the beam, and the sample was placed off the focus plane [see Fig. 1(b)]. The beam waist of the fundamental waves on the surface of the crystal is around 100 µm. The *x*-cut SBN crystal used has the dimensions $6.9 \times 4.6 \times 1$ mm. The optical axis is parallel to the longest axis and the crystal sides are polished to optical quality. The linear input polarization is controlled by a $\lambda/2$-wave plate appropriate to the used wavelength range. The output polarization in turn is analyzed by a suitable analyzer.

We have measured the emission angles for all three processes for different wavelengths and the dependence of Čerenkov SHG intensities on the polarization of the fundamental wave. These results will be presented and discussed in the following section.

## 3. Experimental results and discussion

Figure 1(c) shows three second-harmonic signals of 1200 nm emitted at the Čerenkov angles, excited by a linearly polarized fundamental beam at an angle of 45° with respect to the c-axis.

#247476 Received 6 Aug 2015; revised 25 Sep 2015; accepted 27 Sep 2015; published 21 Oct 2015

In addition to the strong signal in the middle, six intensity maxima, three on every side, emitted under Čerenkov angles are clearly observable. When looking perpendicularly to the optical axis, this random modulation of $\chi^{(2)}$ can be considered as an 1D modulation because of the characteristic elongation of the domains, i.e the large discrepancy in the domain dimensions [see Figs. 2(c) and 2(e)]. Thus, as the domains are much longer in the *z*-direction (tens of micrometers) compared to the *x*-direction (nanometers to a few micrometers) Čerenkov SHG is emitted and modulated mainly along the *x*-axis [see Fig. 1(c)]. The random domain-size dis-

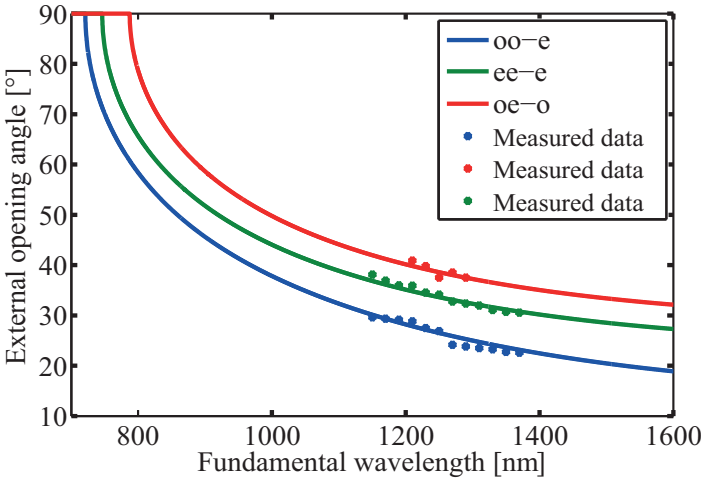


Fig. 3. Measured opening angles in dependence of the wavelength; solid lines representing calculated values from the phase-matching condition [cf. Fig. 1(a)].

tribution leads to a Bragg-phase matched SH signal, emitted over a wide angle. The SH intensity distribution strongly depends on the average domain size [22]. For the cooled-down case, i.e. nanoscaled domains, SH signal is weak and scattered, such that Čerenkov emission is covered and not separable. For microscaled domains, the distribution yields a stronger SH signal localized in directions on the plane perpendicular to the optical axis within 20° from the propagation direction for wavelengths larger than 1 μm [22]. In this case, Čerenkov emission is clearly observable as shown in Fig. 1(c). In combination with each Čerenkov signal at each side, one can also see a color distribution at Čerenkov angle for extraordinarily polarized input beam, from larger wavelength (red) to smaller wavelength (yellow) as a consequence of Čerenkov phase-matching condition. This represents the second harmonics in the visible range of the pulse spectrum. The spectral broadening due to the self-phase modulation is also clearly seen [24]. These different intensity maxima are classified and marked, depending on the polarization of the individual signals. The experiment shows that the outer-SH incomplete ring is the weakest ring. That can be attributed to the fact that the $o+e \rightarrow o$ process has the largest phase mismatch, and thus the weakest intensity. In other words, the transverse phase mismatch is partially compensated by grating vectors of the nonlinear structures. Although the second-order nonlinear coefficients correspond to $o+o \rightarrow e$ and $o+e \rightarrow o$, $d_{15}$ and $d_{31}$ are nearly equal. It is worth to mention here, that the ring could be complete if the domains are modulated in the *z*-axis within the illuminated area. The intensities on the plane perpendicular to the optical axis are still stronger. Now, for deeper analysis the opening angle of the individual rings was measured over a wavelength range as shown in Fig. 3. In general, all Čerenkov signals were weak and not detectable for the case of a cooled-down sample, i.e. small domains. Moreover, the measuring over a wide wavelength range has failed, and especially for the $e+o \rightarrow o$ process, due to low

#247476 Received 6 Aug 2015; revised 25 Sep 2015; accepted 27 Sep 2015; published 21 Oct 2015

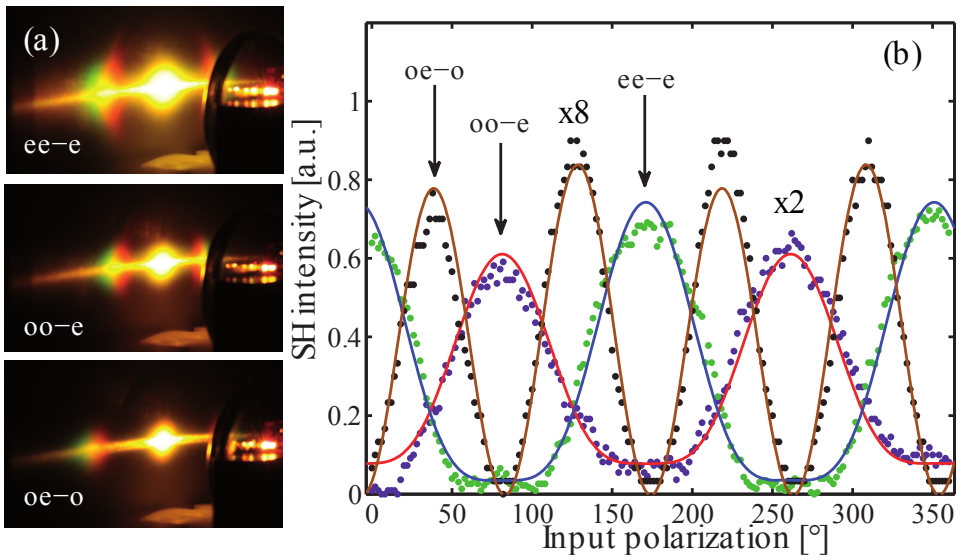


Fig. 4. Analyzing the output polarization of the three Čerenkov-phase matched second harmonics at 1200 nm [see Visualization 3]. In (a) the photographs show each second harmonic filtered by an analyzer. In (b) the experimentally measured SH signals are plotted in dependence of the input polarization angle $\varphi$ for three fixed positions of the analyzer: 0° ($o+o \rightarrow e$ and $e+e \rightarrow e$) and 90° ($o+e \rightarrow o$); the solid lines represent theoretical fits.

laser intensities below 1200 nm and above 1350 nm. However, the measured data are in good agreement with the expected values, which only depend on the refractive indices [25]. The best results were recorded for input wavelengths between 1150 nm and 1370 nm for the $e+e \rightarrow e$ and $o+o \rightarrow e$ processes. The theoretical calculation shows that the total internal reflection of the signals inside the crystal is different for each nonlinear process. For instance, at 800 nm all second harmonics would be transmitted. In contrast, at 700 nm only Čerenkov SHG from $o+o \rightarrow e$ process will leave the crystal.

The $\chi^2$ tensor allows three polarization possibilities for the configuration of propagation perpendicularly to the optical axis. For propagating along the $y$-axis, the corresponding effective second-order nonlinear coefficients are: $d^o_{\text{eff}} = 2d_{15}\sin\varphi\cos\varphi$, $d^e_{31} = d_{31}\sin^2\varphi$, and $d^e_{33} = d_{33}\cos^2\varphi$, where $\varphi$ is the input-polarization angle. Analyzing the output intensity of the individual rings was also performed by using an suitable analyzer behind the sample to separate the rings as can be seen in Fig. 4. The experimental photographs clearly show the positions and the intensity differences of the separated intensity maxima. In the investigated wavelength range $1150-1370$ nm, the extraordinary SH intensity, which is a result from the interaction $e+e \rightarrow e$, is always the strongest component in comparison with the other allowed processes. In the same wavelength range, the ordinarily polarized component exhibits the weakest intensity. For the extraordinary input polarization there is just one SH component $e+e \rightarrow e$, whose intensity maximum is still stronger than the maximum corresponding the other extraordinary component when the input polarization is ordinary. Although the phase-mismatch corresponding the $o+o \rightarrow e$ process is smaller as shown in Fig. 4(a). We think here that the ratio $d_{13}/d_{33}$ is too small to be able to compensate this mismatch difference of the two polarization components. The phase-mismatch becomes more clear when comparing the intensities corresponding the processes $o+o \rightarrow e$ and $o+e \rightarrow o$ while $d_{13}$ and $d_{15}$ are equal. Experimentally measured dependence of the SH intensities vs. the input polarization of the fundamental beam is shown

#247476 Received 6 Aug 2015; revised 25 Sep 2015; accepted 27 Sep 2015; published 21 Oct 2015

in Fig. 4(b). In all these plots, the polarization of the fundamental beam is varied and the lines show the theoretical results. We note a very good agreement between theory and experiment. All Čerenkov maxima are seen at 45° with respect to the optical axis, where SH intensity of the process $e+o \rightarrow o$ reaches its maximum.

We note that cascaded Čerenkov-type third-harmonic generation can also be detected. It is weaker and more complex because there are more possible polarization components which are more difficult to be measured.

## 4. Conclusions

In conclusion, we have studied Type I and II Čerenkov-phase matched SHG in a multidomain SBN crystal. Typically the Čerenkov signals are covered by the broad SH signal that is non-linear Bragg-matched. However, when the size of the laser focus becomes comparable with the domain dimensions, the intensity of Bragg-matched SHG decreases while the intensity of Čerenkov-phase matched SHG increases. When an extraordinary and an ordinary wave propagate perpendicular to the optical axis, all three nonlinear processes ($o+o \rightarrow e$, $e+e \rightarrow e$, and $o+e \rightarrow o$) are Čerenkov-phase matched simultaneously. The Čerenkov opening angles have been measured over a wide wavelength range and the relation of the effective nonlinear coefficients has been determined in dependence of the polarization of the fundamental wave.

## Acknowledgment

Financial support of Deutsche Forschungsgemeinschaft and Open Access Publication Fund of University of Münster is gratefully acknowledged. We also thank Julia Hanisch and Alessandro Zannotti for the fruitful discussions.

#247476 Received 6 Aug 2015; revised 25 Sep 2015; accepted 27 Sep 2015; published 21 Oct 2015